Research Article

A comparative study of energy management systems under connected driving: cooperative car-following case

Ozan Yazar[1], Serdar Coskun[2], Fengqi Zhang[3], Lin Li[4]

[1]Sorgun Vocational School, Department of Transportation Services, Yozgat Bozok University, Yozgat 66700, Turkey.
[2]Department of Mechanical Engineering, Tarsus University, Mersin 33400, Turkey.
[3]School of Mechanical and Precision Instrument Engineering, Xi'an University of Technology, Xi'an 710048, Shaanxi, China.
[4]School of Traffic and Transportation, Northeast Forestry University, Harbin 150040, Heilongjiang, China.

Correspondence to: Dr. Serdar Coskun, Department of Mechanical Engineering, Tarsus University, Takbas Mahallesi Kartaltepe Sokak, Tarsus, Mersin, 33400, Turkey. E-mail: serdarcoskun@tarsus.edu.tr

Abstract

In this work, we propose connected energy management systems for a cooperative hybrid electric vehicle (HEV) platoon. To this end, cooperative driving scenarios are established under different car-following behavior models using connected and automated vehicles technology, leading to a cooperative cruise control system (CACC) that explores the energy-saving potentials of HEVs. As a real-time energy management control, an equivalent consumption minimization strategy (ECMS) is utilized, wherein global energy-saving is achieved to promote environment-friendly mobility. The HEVs cooperatively communicate and exchange state information and control decisions with each other by sixth-generation vehicle-to-everything (6G-V2X) communications. In this study, three different car-following behavior models are used: intelligent driver model (IDM), Gazis–Herman–Rothery (GHR) model, and optimal velocity model (OVM). Adopting cooperative driving of six Toyota Prius HEV platoon scenarios, simulations under New European Driving Cycle (NEDC), Worldwide Harmonized Light Vehicle Test Procedure (WLTP), and Highway Fuel Economy Test (HWFET), as well as human-in-the-loop (HIL) experiments, are carried out via MATLAB/Simulink/dSPACE for cooperative HEV platooning control via different car-following-linked-vehicle scenarios. The CACC-ECMS scheme is assessed for HEV energy management via 6G-V2X broadcasting, and it is found that the proposed strategy exhibits improvements in vehicular driving performance. The IDM-based CACC-ECMS is an energy-efficient strategy for the platoon that saves: (i) 8.29% fuel compared to the GHR-based CACC-ECMS and 10.47% fuel compared to the OVM-based CACC-ECMS under NEDC; (ii) 7.47% fuel compared to the GHR-based CACC-ECMS and 11% fuel compared

to the OVM-based CACC-ECMS under WLTP; (iii) 3.62% fuel compared to the GHR-based CACC-ECMS and 4.22% fuel compared to the OVM-based CACC-ECMS under HWFET; and (iv) 11.05% fuel compared to the GHR-based CACC-ECMS and 18.26% fuel compared to the OVM-based CACC-ECMS under HIL.

Keywords: Hybrid electric vehicles, energy management, equivalent consumption minimization strategy, connected and automated vehicles, car-following models

1. INTRODUCTION

Due to increasing concerns about exhaust emissions and global warming, automotive manufacturers have started to develop environment-friendly vehicles. In this context, hybrid electric vehicles (HEVs) that consume less energy compared to vehicles running on carbon-based fuels are seen as a potential solution. HEVs combine an internal combustion engine (ICE) and one or more electric motors to generate and transmit power to wheels[1–4]. The use of intelligent transportation system (ITS) and vehicle connectivity technologies in HEVs provides great opportunities in reducing energy consumption and emissions[5,6]. Therefore, the utilization of connected and automated vehicle (CAV) technologies along with vehicle-to-everything (V2X) communication, such as vehicle-to-vehicle (V2V) communication and vehicle-to-infrastructure (V2I) communication, reduces reliance entirely on the onboard sensors, which may lead to inaccurate estimations/predictions as well as inefficient driving strategies[7]. Based on these limitations, safety remains a key challenge in developing and commercializing autonomous HEVs. Conversely, cooperative communication via V2X, combined with the onboard sensors, handles the limitations of latency in decision-making and control, resulting in reliable applications. Deployment of V2X communication in the sixth-generation (6G) mobile network (6G-V2X) can increase the knowledge of the environment[8,9], enabling to share the information with the nearby HEVs in addition to onboard sensors; therefore, it better improves vehicle energy efficiency, vehicle performance, driving comfort, and safety[10,11].

HEVs are generally divided into three types: parallel, series, and parallel–series mix (power-split)[12]. In power-split HEVs, electric motor power is provided as additional propulsion to conventional ICEs. This leads to a control design freedom in power-split HEVs. Therefore, in systems with multiple power supplies, a well-designed energy management strategy (EMS) can improve vehicular performance[13]. The purpose of EMS is to control and adjust power distribution between power sources in order to fully optimize fuel consumption, vehicle performance, and emissions[14,15]. EMSs aim not only to divide the required drive power between drive sources but also to maximize the overall efficiency of the vehicle and minimize emissions[16,17]. In connected driving scenarios, an energy management control algorithm is expected to be online adjustable, computationally traceable, and robust to dynamic changes at any time[18]. In this context, a typical instantaneous optimization algorithm is the equivalent consumption minimization strategy (ECMS), which is a real-time energy management control.

ECMS is based on Pontryagin's minimum principle (PMP) and was first proposed by Paganelli for HEVs[19–21]. The main purpose of ECMS is to provide power distribution by minimizing instant equivalent fuel consumption with equivalent factor (EF) in order to convert electricity consumption directly to an equivalent amount of fuel consumption[22,23]. In power-split HEVs, the electric motor gives mechanical power while the battery is discharging[24]. The electrical energy is then converted into an equivalent consumption. If ICE provides mechanical power, the battery is charged. Mechanical energy is taken by ICE, converted into electrical energy, and stored in the battery. This stored electrical energy is used to generate mechanical power in the electric motor. In this way, the power distribution is determined by minimizing the equivalent fuel consumption[14]. Real-time control based on this strategy is useful, and near-optimal results are achieved without knowledge of the entire driving cycle, thus providing an advantage for real-time applications in connected energy manage-

ment systems[25].

The EMS can be solved under connected driving scenarios to minimize global energy consumption[26,27]. Many studies have been conducted on using front car information in EMS design to increase the energy efficiency of HEVs. These studies mainly focus on the car-following models to obtain vehicle information ahead. In regards to the car-following models, the literature goes back more than fifty years[28,29]. Since then, many mathematical models have been developed, mainly to determine driver behavior and vehicle stability in traffic flow, e.g., the intelligent driver model (IDM), Gazis–Herman–Rothery model (GHR), and optimal velocity model (OVM)[30–32]. IDM, GHR, and OVM are types of microscopic traffic flow car-following models, in which the decision of any driver to accelerate or brake depends only on the position and the speed of the vehicle ahead. Using the idea of car-following models, automated vehicle control technologies have drawn great attention, and adaptive cruise control (ACC) emerged. ACC tries to imitate the driver's behavior to eliminate the potential dangers that may arise from the driver such as the driver's reaction time and misperception. The ACC system adjusts vehicle motion by maintaining a safe distance from the vehicle ahead of it in the same lane[33,34]. The distance between the vehicle and the relative speed is measured by sensors, and ACC controls the throttle and brakes for a follower vehicle, as shown in Figure 1. With the development of communication technologies (such as V2V), cooperative adaptive cruise control (CACC) emerged as an extension of ACC, which has the ability of vehicle coordination and cooperation under platooning. Similar to the ACC system, communication-enabled CACC regulates the vehicle speed to maintain a safe distance gap and the user-desired relative velocity. These automated vehicle systems are developed to improve energy savings and traffic safety by optimizing speed trajectories that can be incorporated with the EMS to further boost fuel economy. In terms of energy management in car-following modes, the authors of[27,35,36] addressed the safe distance gap and the relative speed with respect to the movement of the vehicle ahead to improve fuel economy and safety. A model predictive control (MPC)-based ACC has been proposed considering traffic rules and road conditions in a car-following scenario[37]. Few studies have focused on the optimization of internal powertrain energy management with the consideration of interactions between multiple vehicles under platooning. Multiple HEVs' energy optimization has been studied considering external driving coordination, and a fuel-saving of 17.9% is achieved compared with a baseline counterpart[38]. A distributed cooperative energy management control incorporating driving behavior and vehicle state information has been proposed for plug-in HEVs[39]. A nonlinear MPC to minimize the energy consumption of a group of fuel cell vehicles platoon considering V2V communication has been proposed[40]. Simulation results demonstrate 16.1%, 6.2%, and 11.7% improvements of energy under UDDS, HWFET, and NEDC drive cycles, respectively. A control method for homogeneous vehicle platoon energy consumption minimization while ensuring the string stability has been studied[41]. Based on an energy-oriented spacing strategy, the energy consumption of the platoon is reduced by 7.3% and 5.7%, compared to a constant spacing and constant time headway policy.

The potential impacts of CACC on traffic safety and HEV energy efficiency are a promising field of study because CACC vehicles are expected to penetrate the market more in the near future, and cooperative communication of HEVs with the nearby HEVs using 6G-V2X communication can boost global fuel-saving and traffic safety. Although the aforementioned works contribute to the research in the development of EMSs for HEVs under platooning, there is still a lack of thorough comparative study of the car-following models for fuel efficiency and traffic safety under cooperative driving scenarios. To this end, the following contributions are made: (a) A comparative investigation of IDM, GHR, and OVM microscopic traffic flow models is utilized under connected and cooperative driving scenarios to demonstrate their potential impacts on global energy savings for HEVs; (b) The proposed ECMS is used to further explore the capacity of energy-saving potential of HEVs in a platoon by incorporating the CACC coordinated traffic information in a fuel optimal manner; (c) Extensive simulation studies are carried out under New European Driving Cycle, Worldwide Harmonized Light Vehicle Test Procedure, Highway Fuel Economy Test, and human-in-the-loop drive cycles to clearly demonstrate the advantages of cooperative HEV platooning control methods in terms of speed deviations,
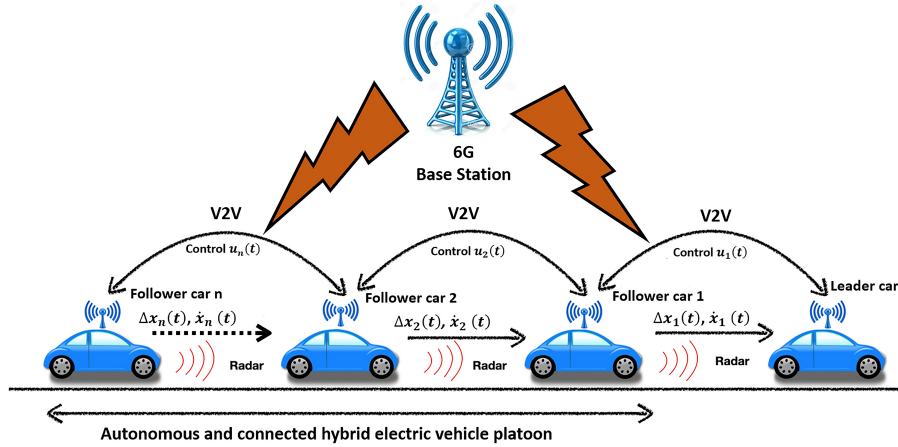
Figure 1. Schematic representation of the CACC system is shown.

battery charge sustainability, and fuel economy.

The rest of the paper is structured as follows. Section 2 presents the control-oriented powertrain model for HEVs along with power flow management. Section 3 introduces the car-following models and Section 4 explains the design of cooperative platoon formation for automated and connected HEVs using car-following models. Extensive simulation studies are demonstrated in Section 5. Lastly, conclusions and future research directions are given in Section 6.

2. ENERGY MANAGEMENT PROBLEM FORMULATION

2.1. Internal Combustion Engine Model

Since the internal combustion engine is a complex system that includes many components, an experimental dataset as a function of engine speed and engine torque is used in this study. The engine speed and torque express the engine fuel consumption ratio by Equations (1), and Equation (2) denotes the engine torque as follows.

$$\dot{m}_{fuel}(t) = f(T_e(t), n_e(t)) \tag{1}$$

$$T_e(t) = \alpha(t).T_{emax}(n_e(t)) \tag{2}$$

where $n_e(t)$ denotes the engine speed, $T_e(t)$ denotes the engine torque, $\alpha(t)$ is the engine throttle, and $T_{emax}(n_e(t))$ is the engine maximum torque at the current engine speed.

2.2. Electric Motor Model

The purpose of electric motor (EM) modeling is to obtain the motor power based on motor speed. By ignoring the effect of the dynamic properties of the EM, Equation (3) expresses the efficiency of the motor as a function of the motor speed and motor torque. Then, the required engine power is defined by Equation (4).
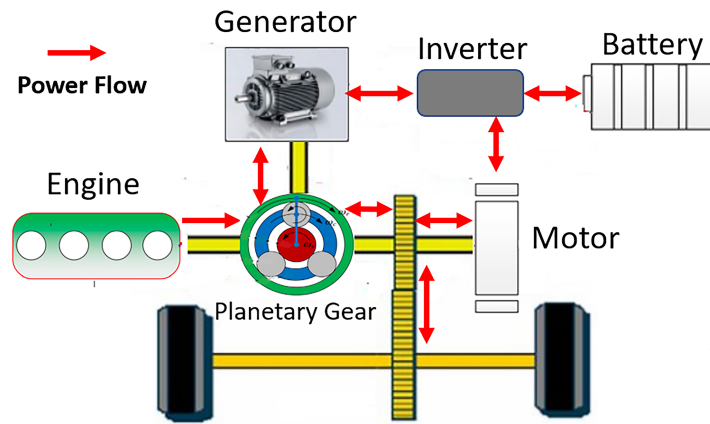
$$\eta_m = \Psi(T_m(t), (n_m(t)) \tag{3}$$

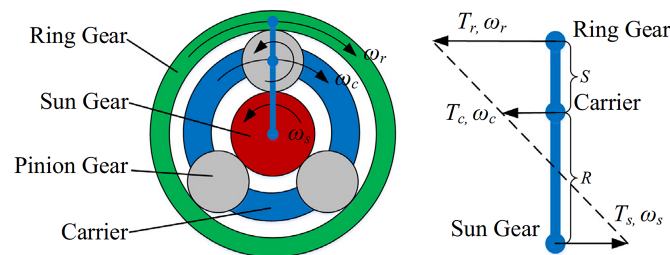**Figure 2.** Structure of power-split hybrid electric vehicles [14].

Figure 3. Structure and lever diagram of the planetary gear system equipped in a power-split HEV.

$$P_m(T_m(t),(n_m)(t)) = \begin{cases} \frac{T_m\,n_m}{9550\eta_m}, & T_m > 0, \\ \frac{T_m\,n_m\,\eta_m}{9550}, & T_m \leq 0. \end{cases} \tag{4}$$

where $n_m(t)$ denotes the motor speed, $T_m(t)$ denotes the motor torque, η_m is the motor efficiency, and $P_m(t)$ is the required motor power (kW).

2.3. Control-Oriented Powertrain Model

Taking advantage of the mixed powertrain configuration (both series and parallel)[42], a power-split HEV model of Toyota Prius is adopted in this study. This HEV powertrain model has been successfully used and commercialized as it has the advantages of the mixed configuration[43,44]. The power-split HEV model is shown in Figure 2.

The whole powertrain components of the power-split HEV include one engine, generator/motor (M/G1 and M/G2). The planetary gear set implementation achieves power splitting functionality where the engine is connected to the planet carrier, M/G1 is connected to the sun gear, and a torque coupler is used to combine the ring gear with the M/G2 to power the final drive[45,46]. Figure 3 shows the structure of the planetary gear system. The kinematic equation of the gear system can be derived as the angular velocities of the sun gear, ring gear, and planet carrier.

$$\omega_s(t)\,S + \omega_R(t)\,R = \omega_c(t)\,(S + R) \tag{5}$$

where the radius of the sun gear and the ring gear are denoted by S and R, respectively. Angular velocities of sun, ring, and carrier are given by $\omega_S(t)$, $\omega_R(t)$, and $\omega_C(t)$, respectively. If we assume that all powertrain shafts are rigid and neglect the pinion gears inertia, the powertrain dynamics can be expressed as follows:

$$I_{M/G1}\frac{d\omega_{M/G1}}{dt} = T_{M/G1}(t) + FS \tag{6}$$

$$I_{eng}\frac{d\omega_{eng}}{dt} = T_{eng}(t) - F(S+R) \tag{7}$$

$$I_{M/G2}\frac{d\omega_{M/G2}}{dt} = T_{M/G2}(t) - \frac{T_{axle}(t)}{g_f} + FR \tag{8}$$

where the inertias of the generator, engine, and motor are denoted by $I_{M/G1}$, I_{eng}, and $I_{M/G2}$, respectively; the engine torque is $T_{eng}(t) = T_C(t)$; $M/G1$ torque is $T_{M/G1}(t) = T_S(t)$; and $M/G2$ torque is $T_{M/G2}(t) = T_R(t)$. The internal force on pinion gears is F, the gear ratio of the final drive is g_f, and the produced torque from powertrain on the drive axle is $T_{axle}(t)$. To benefit of the control-oriented model in energy optimization, the steady-state values are used of the left-hand in Equations (6)–(8), leading to the following $M/G2$ torque and vehicle velocity equations

$$\omega_{M/G2}(t) = \frac{g_f}{R_{wheel}}V \tag{9}$$

$$m\frac{dV}{dt} = T_{axle}(t) + T_{brake}(t) - mg\sin(\theta(t)) - \frac{1}{2}\rho AC_d V^2 - C_r mg\cos(\theta(t)) \tag{10}$$

where R_{wheel} is the radius of wheel, V denotes the longitudinal velocity of the vehicle, the vehicle mass is denoted by m, the friction brake torque is $T_{brake}(t)$, g is the gravitational acceleration, and $\theta(t)$ is the road grade, which is assumed to be zero in this study. $\frac{1}{2}\rho AC_d V^2$ denotes the aerodynamic drag resistance and C_d is the rolling resistance coefficient. A well-designed EMS seeks to compute optimal power split between the internal combustion engine and electric motor/generator to minimize energy consumption at each time instant of the solution. Assuming that the engine is in optimal operating condition and the dynamic characteristics are ignored, then the engine fuel rate $\dot{m}_{fuel}$ and operational efficiencies of $M/G1$ and $M/G2$ ($\eta_{M/G1}$ and $\eta_{M/G2}$) are extracted from empirical data as functions of angular velocities and torques as follows:

$$\dot{m}_{fuel}(t) = \Psi_{eng}(\omega_{eng}(t), T_{eng}(t)) \tag{11}$$

$$\eta_{M/G1}(t) = \Psi_{M/G1}(\omega_{M/G1}(t), T_{M/G1}(t)) \tag{12}$$

$$\eta_{M/G2}(t) = \Psi_{M/G2}(\omega_{M/G2}(t), T_{M/G2}(t)) \tag{13}$$

where empirical data for the engine, generator, and motor are Ψ_{eng}, $\Psi_{M/G1}$, and $\Psi_{M/G2}$, respectively. A battery in a power-split HEV is used to supply or recover energy from electricity via an inverter. A fundamental battery resistance model is utilized to describe the battery[47,48]. Then, the battery charge sustainability, i.e., state of charge (SOC), is calculated as:

$$\dot{SOC}(t) = -\frac{I_{batt}(t)}{Q_{max}} \tag{14}$$

$$P_{batt}(t) = V_{oc}I_{batt}(t) - I_{bat}(t)^2 R_{batt} \tag{15}$$

where $I_{batt}(t)$ denotes the battery current, Q_{max} is the maximum capacity of battery, $P_{batt}(t)$ denotes the battery power, R_{batt} is the internal resistance, and V_{oc} is the the open circuit voltage. Then, the following equation expresses the terminal battery power requirement:

Table 1. Main parameters of power-split hybrid electric vehicle [49,50]

Component	Parameter	Value
Internal Combustion Engine	Type	Four-cylinder in-line gasoline engine
	Maximum power	57 kW @ 4500 RPM
	Maximum torque	110 Nm @ 4500 RPM
Electric motor	Type	AC motor
	Maximum power	35 kW @ 1040-5600 RPM
	Maximum torque	30 kW @ 3000-5500 RPM
Battery	Energy capacity	5 kWh/battery pack
	Charging capacity	2.3 Ah/battery unit
	Battery cell layout	110 serial × 6 parallel

$$P_{batt} = P_{M/G1}(t)/(\eta_{M/G1}(t).\eta_{inv}(t))^{k_{M/G2}(t)} + P_{M/G2}(t)/(\eta_{M/G2}(t).\eta_{inv}(t))^{k_{M/G2}(t)} \tag{16}$$

where $P_{M/G1}(t)$ and $P_{M/G2}(t)$ are shaft powers and η_{inv} is the inverter efficiency.

$$k_i(t) = \begin{cases} 1 & \text{if} \quad P_i(t) > 0 \\ -1 & \text{if} \quad P_i(t) < 0 \end{cases} \quad , \quad \text{for} \quad i = \{M/G1\}, \{M/G2\} \tag{17}$$

Equations (5)–(17) explains the energy management-oriented model used in this paper. The main parameters of the power-split hybrid electric vehicle are given in Table 1.

2.4. Equivalent consumption minimization

Taking advantage of a real-time energy optimization strategy, ECMS does not require entire driving cycle information in advance, and, by converting electricity consumption to equivalent fuel consumption as well as considering the constraints in engine, motor, generator, and battery, instantaneous equivalent fuel consumption is minimized. To this end, the equivalent factor (EF) is required to convert the electricity consumption into equivalent fuel consumption. The general formulation for the above-mentioned problem is given below.

$$\dot{m}_{eqv}(a(t), t) = \dot{m}_f(a(t), t) + \dot{m}_e(a(t), t)$$

$$= \dot{m}_f(a(t), t) + s(t) \frac{P_m(a(t), t)}{Q_{LHV}} \tag{18}$$

$$\left[T_{eng_{opt}}(t), T_{M/G1_{opt}}(t), T_{M/G2_{opt}}(t)\right] = Min(\dot{m}_{eqv}) \tag{19}$$

subject to

$$\omega_{eng}^{min} \leq \omega_{eng}(t) \leq \omega_{eng}^{max} \tag{20}$$

$$\omega_{M/G1}^{min} \leq \omega_{M/G1}(t) \leq \omega_{M/G1}^{max} \tag{21}$$

$$\omega_{M/G2}^{min} \leq \omega_{M/G2}(t) \leq \omega_{M/G2}^{max} \tag{22}$$

$$T_{eng}^{min} \leq T_{eng}(t) \leq T_{eng}^{max} \tag{23}$$

$$T_{M/G1}^{min} \leq T_{M/G1}(t) \leq T_{M/G1}^{max} \tag{24}$$

$$T_{M/G2}^{min} \leq T_{M/G2}(t) \leq T_{M/G2}^{max} \tag{25}$$

$$I_{batt}^{min} \leq I_{batt}(t) \leq I_{batt}^{max} \tag{26}$$

$$P_{batt}^{min} \leq P_{batt}(t) \leq P_{batt}^{max} \tag{27}$$

$$SOC^{min} \leq SOC(t) \leq SOC^{max} \tag{28}$$

where $a(t)$ is the control input, $\dot{m}_{eqv}(t)$ denotes the equivalent fuel consumption, $\dot{m}_f(t)$ is the engine fuel consumption (kg/s), $\dot{m}_e(t)$ is the equivalent fuel consumption (kg/s), $s(t)$ is the equivalent factor, $\omega_{eng}(t)$ is the engine angular speed (rpm) with minimum ω_{eng}^{min} and ω_{eng}^{min} values, $\omega_{M/G1}(t)$ is the $M/G1$ angular speed (rpm) with minimum $\omega_{M/G1}^{min}$ and maximum $\omega_{M/G1}^{max}$ values, $\omega_{M/G2}(t)$ is the $M/G2$ angular speed (rpm) with minimum $\omega_{M/G2}^{min}$ and maximum $\omega_{M/G2}^{max}$ values, $T_{eng}(t)$ is the engine torque (Nm) with minimum T_{eng}^{min} and maximum T_{eng}^{max} values, $T_{M/G1}(t)$ is the $M/G1$ torque (Nm) with minimum $T_{M/G1}^{min}$ and maximum $T_{M/G1}^{max}$ values, $T_{M/G2}$ is the $M/G2$ torque (Nm) with minimum $T_{M/G2}^{min}$ and maximum $T_{M/G2}^{max}$ values, $P_{batt}(t)$ is the battery power (kW) with minimum P_{batt}^{min} and maximum P_{batt}^{max} values, and $I_{batt}(t)$ is the battery current with minimum I_{batt}^{min} and I_{batt}^{min} maximum values. At each time step of the simulation, the cost function in Equation (18) is minimized by satisfying the constraints in Equations (20)–(28).

3. CAR-FOLLOWING MODELS

A car-following model is used to control the driver's behavior, such as maintaining a safe distance and desired reference velocity tracking considering the vehicle ahead in traffic. The following vehicle adjusts its speed according to the preceding vehicle for comfortable driving and safe braking distance[51]. Although the follower's action is usually specified through its acceleration, in some models, the follower's action is defined with the follower's speed[52]. Meanwhile, car-following models use different formulas to describe the follower's behavior. In this work, we introduce three different types of car-following models for the most basic driving behavior to construct reliable models for the development of energy management problems of HEVs under connected driving.

3.1. Intelligent Driver Model

The Intelligent Driver Model (IDM) was developed by Treiber, Hennecke, and Helbing in 2000, which is a type of adaptive cruise control system designed to set the desired longitudinal speed and safety time interval of the driver. It is a type of car-following model that can adjust the driver's behavior according to the changing traffic. To this end, in the IDM, the follower vehicle acceleration varies depending on the distance and speed of the preceding vehicle. In the IDM, the nth vehicle acceleration at time t is defined below[30].

$$\ddot{x}_n(t) = a. \left[1 - \left(\frac{\dot{x}_n(t)}{\dot{x}_0} \right)^{\delta} - \left(\frac{s^*(\dot{x}_n(t), \Delta\dot{x}_n(t))}{s_n(t)} \right)^2 \right] \tag{29}$$

where $\ddot{x}_n(t)$ is the acceleration of the nth vehicle, $\dot{x}_n(t)$ is the speed of the nth vehicle, a is the follower vehicle's maximum acceleration, δ is the exponent for vehicle's acceleration, $\dot{x}_0$ is the desired velocity of the nth vehicle, $\Delta\dot{x}_n(t)$ is the relative velocity of the follower vehicle with its preceding vehicle (i.e., $\Delta\dot{x}_n(t) = \dot{x}_{n-1}(t) - \dot{x}_n(t)$), and s_n is the distance gap (m) distance between nth and $(n-1)$th vehicle, defined as

$$s_n(t) = \Delta x_n(t) - l_n \tag{30}$$

where $\Delta x_n(t)$ is the distance between the follower vehicle and the vehicle in front of it, i.e., $\Delta x_n(t) = x_{n-1}(t) - x_n(t)$, and l_n is vehicle length. The desired minimum gap of the nth vehicle, s_n^*, is given by

$$s^*(\dot{x}_n(t), \Delta x_n(t)) = s_0 + \max \left[0, \left(\dot{x}_n(t)T + \frac{\dot{x}_n(t)\Delta\dot{x}_n(t)}{2\sqrt{ab}} \right) \right] \tag{31}$$

where b denotes the nth vehicle maximum deceleration and T is the safe time headway (s). s_0 denotes the minimum space headway between nth vehicle and $(n-1)$th vehicle (ahead of the nth vehicle). In the IDM, acceleration divides the vehicle into two parts. In the model, (a) is the maximum acceleration that the vehicle can achieve with free flow velocity and (b) is the comfortable braking deceleration. In this context, $\ddot{x}_n(t)$ can be divided into sections; the first part $(1 - \left(\frac{\dot{x}_n}{\dot{x}_0}\right)^\delta)$ indicates the required acceleration depending on the desired speed, while the second part $\left(\frac{s^*(\dot{x}_n, \Delta\dot{x}_n)}{s_n}\right)^2$ indicates the required deceleration depending on the desired gap between the nth vehicle and $(n-1)$th vehicle. The second part is valid if the distance Δx_n between nth vehicle and $(n-1)$th vehicle is less than the desired distance.

The desired distance s^* between the nth vehicle and $(n-1)$th vehicle consists of the minimum stopping distance s_0 and the speed-dependent distance $\dot{x}_n T$. This corresponds to preceding vehicle in front of the follower vehicle in flowing traffic conditions in the desired T time interval. In this braking situation, the vehicle can be decelerated comfortably depending on the maximum deceleration b.

3.2. Gazis–Herman–Rothery (GHR) Model

The GHR model, also known as the General Motors (GM) model, is developed by Gazis–Herman–Rothery in the 1950s. The GHR model is a stimulus-based car following model[31]. GHR model assumes that the following vehicle responds to arbitrarily small changes in relative speed. GHR model also considers that the follower vehicle responds to the actions of the preceding vehicle, even though the distance to the preceding vehicle is very large, and the follower vehicle's response vanishes as the relative velocity is zero. In the GHR model, the acceleration of the follower vehicle, i.e., nth vehicle, is proportional to the speed of the preceding vehicle, i.e., $(n-1)$th, the speed between the nth vehicle and the $(n-1)$th vehicle, and the distance between them[53]. According to the GHR model, the nth vehicle acceleration at time t is calculated below[31].

$$\ddot{x}_n(t) = c\dot{x}_n^m(t) \cdot \frac{\Delta\dot{x}_n(t-T)}{\Delta x^l_n(t-T)} \tag{32}$$

where $\ddot{x}_n(t)$ denotes the acceleration of the nth vehicle, $\dot{x}_n(t)$ denotes nth vehicle speed, $x_n(t)$ is the position of the nth vehicle, $\Delta\dot{x}_n(t)$ is the speed difference between the nth vehicle and the $(n-1)$th vehicle, $\Delta x_n(t)$ is the distance between the following vehicle and the preceding vehicle, and T is the vehicle's reaction time. c, m, and l are model control parameters. Coefficient m shows the extent of the speed of nth vehicle. This can affect the acceleration applied by the driver of the nth vehicle at time t. The constant l indicates how much the distance Δx_n between the follower and the followed vehicles contributes to the acceleration. Moreover, T reaction time is related with c sensitivity constant. These parameters were obtained as a result of experimental studies.

3.3. Optimal Velocity Model

The Optimal Velocity Model (OVM) is a dynamic equation-based car-following model developed by Bando, Hasebe, Nakayama, and Shibata in 1955. According to the OVM, the movement of the vehicle is controlled by an optimal speed. Therefore, in the OVM, the acceleration of the vehicle is calculated based on the difference between the optimal speed and the speed of the vehicle. In the OVM, the acceleration of the nth vehicle at time t is defined by the formula below[32].

$$\ddot{x}_n(t) = k\{V(\Delta x_n(t)) - \Delta\dot{x}_n(t)\} \tag{33}$$

where $\ddot{x}_n(t)$ denotes the nth vehicle acceleration, $\Delta x_n(t)$ is the space headway between the follower vehicle and the followed (preceding) vehicle (i.e., $\Delta x_n(t) = x_{n-1}(t) - x_n(t)$), $\dot{x}_n(t)$ is the speed of the nth vehicle, k is the driver sensitivity and is given by inverse of the delay time, and $V(\Delta x_n(t))$ is the optimal speed function of the nth vehicle, which is given by

Table 2. The values of the parameters used in the vehicle following models

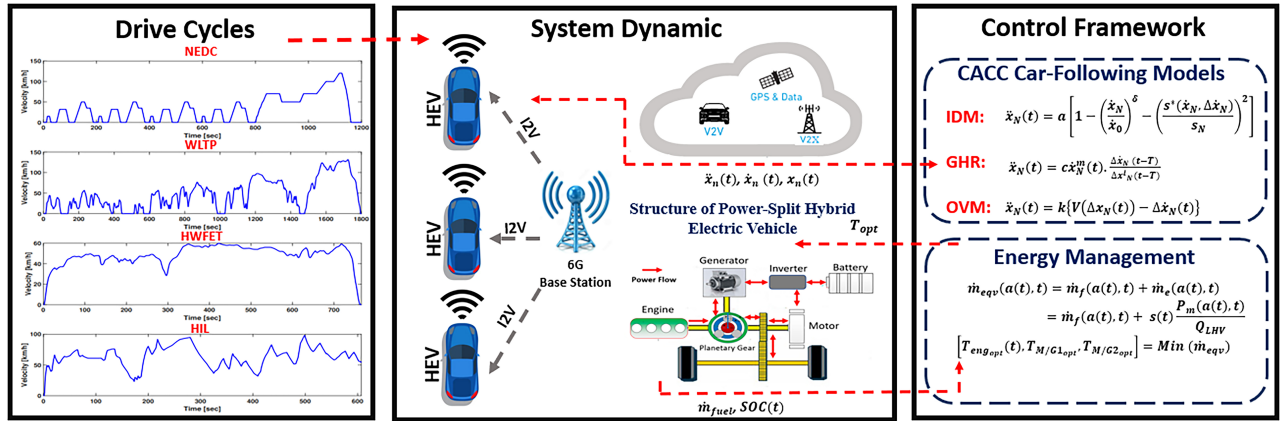| Model	Parameter and values
IDM	$(\dot{x}_0, \delta, a, b, l_n, T, s_0) = (30, 4, 1, 1.5, 1.6, 2, 5)$
GHR	$(c, m, l) = (125, 0.2, 1.6)$
OVM	$(V_1, V_2, C_1, C_2, k, l_n) = (6.75, 7.91, 0.13, 1.57, 0.86, 5)$

Figure 4. Control hierarchy of the proposed approaches.

$$V(\Delta x_n(t)) = V_1 + V_2 . \tanh[C_1(\Delta x_n(t) - l_m) - C_2] \qquad (34)$$

where l_n is the vehicle length, V_1 and V_2 are independent variables, and C_1 and C_2 are constants. These parameters are obtained as a result of experimental studies. In the OVM car-following model, the optimal speed $(V(\Delta x_n(t)))$ is a function of the space headway that denotes the distance between the follower vehicle and the vehicle ahead of it. Based on this function, the acceleration value of the OVM is adjusted to avoid collisions between vehicles.

The values of the above-mentioned models are shown in Table 2 [54,55].

4. CACC PLATOON EXTENSION OF CAR-FOLLOWING MODELS

As an advanced driver assistance system, ACC helps vehicles follow the leading vehicle at a predefined gap by adjusting the vehicle velocity. CACC is an extension of ACC using wireless communication between connected traffic vehicles in a platoon. Connectivity in a CACC system allows vehicles to react more quickly to instantaneous changes than drivers in an ACC system. Furthermore, a CACC system greatly improves safety and mobility in the case of driver distractions and types, and it decreases the negative environmental impacts of emissions. With the help of reliable connectivity between vehicles, CACC enables the execution of appropriate energy management control strategies for HEVs by reducing driver's tasks. To implement classical car-following behavior models under a CACC platoon, we develop a system-level approach to the car-following models that allow adjustment of the vehicle's speed and minimum headway simultaneously with respect to the vehicular state data from multiple vehicles in the CACC platoon. The main underlying idea is that each vehicle in the platoon can react simultaneously to the leader's speed while considering the information of the preceding vehicle [56] in the platoon. For instance, in a platoon of one leader and six follower vehicles, the first following vehicle receives the state information (position, velocity, and acceleration) of the leader in the platoon; likewise, the first follower behaves as a leader vehicle for the vehicle immediately behind and receives the new leader information in real-time. Based on this, the follower vehicles adjust their own state based on the

immediately received information of the preceding vehicle in the platoon. As an emerging technology, in the 6G-V2X environment, vehicles can obtain a massive amount of traffic information where CACC vehicles can be coordinated to improve traffic flow efficiency and throughput as well as energy. The closed-loop system of this research is illustrated in Figure 4. In this work, we adopt three commonly used car-following models in the development of a CACC system for HEVs. The proposed scheme can be employed using ordinary differential equations under a platoon of N vehicles transformation for different car-following behavior models via CACC connectivity characteristics.

4.1. IDM

In the IDM, the follower vehicle acceleration depends on the speed and position of the vehicle in front of it. With the help of the following quadratic ordinary differential equation formulations, the IDM car-following model is converted to a CACC-based model for N vehicles.

$$\ddot{x}_1(t) = a.\left[1 - \left(\frac{\dot{x}_1(t)}{\dot{x}_0}\right)^{\delta} - \left(\frac{s^*(\dot{x}_1(t), \Delta\dot{x}_1(t))}{s_1(t)}\right)^2\right]$$

$$\ddot{x}_2(t) = a.\left[1 - \left(\frac{\dot{x}_2(t)}{\dot{x}_0}\right)^{\delta} - \left(\frac{s^*(\dot{x}_2(t), \Delta\dot{x}_2(t))}{s_2(t)}\right)^2\right]$$

$$\ddot{x}_3(t) = a.\left[1 - \left(\frac{\dot{x}_3(t)}{\dot{x}_0}\right)^{\delta} - \left(\frac{s^*(\dot{x}_3(t), \Delta\dot{x}_3(t))}{s_3(t)}\right)^2\right] \qquad (35)$$

$$\vdots$$

$$\ddot{x}_N(t) = a.\left[1 - \left(\frac{\dot{x}_N(t)}{\dot{x}_0}\right)^{\delta} - \left(\frac{s^*(\dot{x}_N(t), \Delta\dot{x}_N(t))}{s_N(t)}\right)^2\right]$$

where

$$s^*(\dot{x}_N(t), \Delta x_N(t)) = s_0 + \max\left[0, \left(\dot{x}_N(t)T + \frac{\dot{x}_N(t)\Delta\dot{x}_N(t)}{2\sqrt{ab}}\right)\right] \qquad (36)$$

$$s_N(t) = \Delta x_N(t) - l_N \qquad (37)$$

that is

$$\ddot{x} = f(\dot{x}, x, p) \qquad (38)$$

where
$\ddot{x} = (\ddot{x}_1, \ddot{x}_2, \ddot{x}_3...\ddot{x}_N)^T$
$\dot{x} = (\dot{x}_1, \dot{x}_2, \dot{x}_3...\dot{x}_N)^T$
$x = (x_1, x_2, x_3...x_N)^T$
where p is the IDM parameter vector. Equation (38) describes a system of ordinary differential equations for a platoon of N vehicles where all the CACC vehicles' motion can be captured with the use of the IDM car-following behavior.

4.2. GHR

In the GHR, the acceleration of the follower vehicle depends on the speed and position of the vehicle in front of it. With the help of the following quadratic ordinary differential equation formulations, the OVM car-following model is converted to a CACC-based model for N vehicles as follows.

$$\ddot{x}_1 (t) = c\dot{x}_1^m (t) . \frac{\Delta \dot{x}_1 (t - T)}{\Delta x_1^l (t - T)}$$

$$\ddot{x}_2 (t) = c\dot{x}_2^m (t) . \frac{\Delta \dot{x}_2 (t - T)}{\Delta x_2^l (t - T)}$$

$$\ddot{x}_3 (t) = c\dot{x}_3^m (t) . \frac{\Delta \dot{x}_3 (t - T)}{\Delta x_3^l (t - T)} \tag{39}$$

$$\vdots$$

$$\ddot{x}_N (t) = c\dot{x}_N^m (t) . \frac{\Delta \dot{x}_N (t - T)}{\Delta x_N^l (t - T)}$$

Then, the system of differential equation of N vehicles in the CACC platoon becomes

$$\ddot{x} = f (\dot{x}, x, p) \tag{40}$$

where
$$x = (x_1, x_2, x_3...x_N)^T$$
where p is the GHR parameter vector. In Equation (40), $\dot{x}$ and x present the velocities and positions of the CACC vehicles, as well as with the p parameter vector of GHR, respectively.

4.3. OVM
In the OVM, the acceleration of the follower vehicle depends on the speed and position of the vehicle in front of it. With the help of the following quadratic ordinary differential equation formulations, the OVM car-following model is converted to a CACC-based model for N vehicles.

$$\ddot{x}_1 (t) = k \{V (\Delta x_1 (t)) - \Delta \dot{x}_1 (t)\}$$

$$\ddot{x}_2 (t) = k \{V (\Delta x_2 (t)) - \Delta \dot{x}_2 (t)\}$$

$$\ddot{x}_3 (t) = k \{V (\Delta x_3 (t)) - \Delta \dot{x}_3 (t)\} \tag{41}$$

$$...$$

$$\ddot{x}_N (t) = k \{V (\Delta x_N (t)) - \Delta \dot{x}_N (t)\}$$

where

$$V (\Delta x_N(t)) = V_1 + V_2 . \tanh [C_1 (\Delta x_N(t) - l_c) - C_2] \tag{42}$$

The system of differential equations of N vehicles in a CACC platoon becomes

$$\ddot{x} = f (\dot{x}, x, p) \tag{43}$$
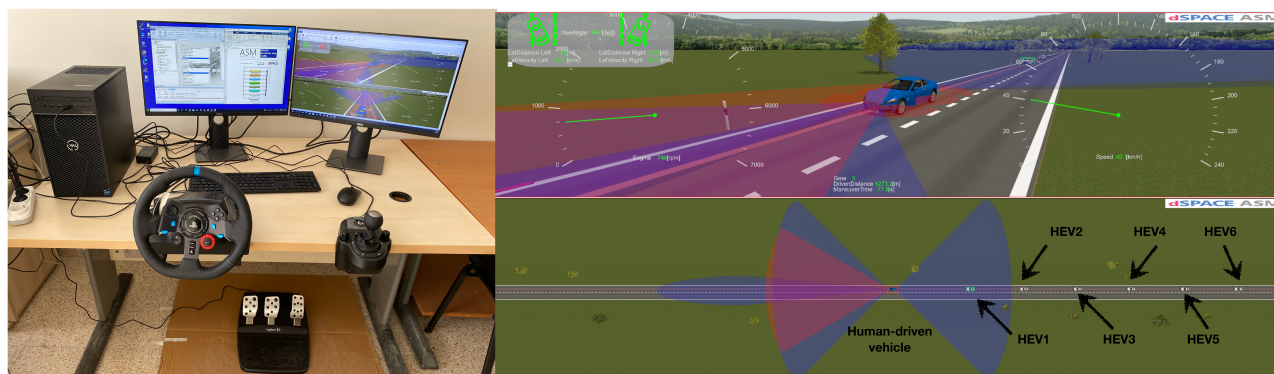
where
$$x = (x_1, x_2, x_3...x_N)^T$$

Figure 5. Real-time experiment using RTI1006 version of dSPACE program, available at http://lab.tarsus.edu.tr/cars. dSPACE is a high-fidelity driving simulator that offers several block sets for testing and validating vehicle control algorithms. The experiments were performed on a computer equipped with an Intel *Xeon 3.2 GHz* CPU. A virtual world of traffic is visually seen on the Motion desk platform of dSPACE that runs on a Simulink model where all the algorithms are packed. For the experiments, a driver is in charge of the leader car (human-driven vehicle) and the following HEVs are connected under CACC car-following behavior models.

p is the OVM parameter vector. Similar to the previous derivations, the vector of positions and speeds of N vehicles CACC platoon are expressed in Equation (43). With the current format, all of the car-following models are packed into a set of differential equations, allowing to develop a system-level model of traffic dynamics.

5. EXPERIMENT RESULTS

Experiments of a homogeneously connected HEV platoon consisting of one leader and six followers were performed to validate the performance of the energy management algorithms under CACC car-following models to demonstrate the reference velocity trajectory performance and fuel economy advantage. The homogeneous platoon refers to all HEVs having the same powertrain parameters in the platoon. The proposed CACC car-following algorithms were written in MATLAB's embedded function blocks and were run online in Simulink with the ECMS algorithm, forming the CACC-ECMS scheme. The leader vehicle exchanges its state information with the follower vehicles in the connected vehicle platoon via 6G-V2X communication. As for the communication topology in the platoon, vehicles are interconnected via predecessor-following communication topology, meaning that followers receive the state information from their preceding vehicles. It is assumed that the CACC-ECMS scheme works on the 6G-V2X network environment, in which the HEVs are considered to travel on a single-lane road. The 6G base station provides network services to the HEVs where each HEV in the CACC-ECMS scheme communicates with the base station to receive target traffic states such as reference velocities, as shown in Figure 1. To ensure traffic safety and fuel efficiency while cruising in the lane, the HEVs compute control inputs and transmit the inputs by cooperative communication. The HEVs in the CACC-ECMS method employ the ultra-low-latent 6G-V2X communication and periodically broadcast the vehicles' state data, such as relative speeds and the gaps between HEVs.

The proposed CACC-ECMS control strategy is examined under four different types of driving conditions, i.e., NEDC, WLTP, HWFET, and HIL drive cycles. NEDC is a driving cycle that represents the typical use of a car in Europe, consisting of four repeated urban driving cycles and one extra-urban driving cycle. NEDC lasts 1200 s, and the vehicle can accelerate to a maximum speed of 120 km/h. The total distance covered in this driving cycle is 11.01 km. WLTP represents a driving cycle compatible with the world average driving conditions for light vehicles. In WLTP, the driving cycle is 1800 s, and the vehicle can accelerate to a maximum speed of 131.33 km/h. The total distance covered in this driving cycle is 23.25 km. HWFET represents a driving cycle for light vehicles that provide fuel economy on the highway. The HWFET driving cycle lasts 765 s, in which the vehicle accelerates to a maximum speed of 60 km/h. The total distance covered in this driving cycle is
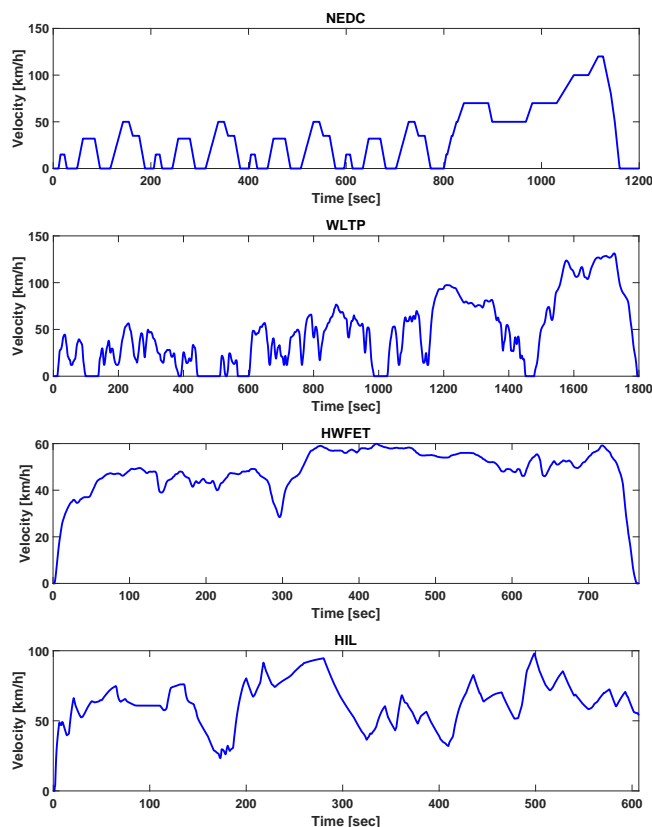
Figure 6. Velocity profile of the driving cycles.

16.45 km. The HIL driving cycle consists of 600 s, in which the driver accelerates to a maximum speed of 98 km/h. The total distance covered in this driving cycle is 11.66 km. The HIL profile is obtained through the setup, as given in Figure 5. The speed profiles of the NEDC, WLTP, HWFET and HIL driving cycles are given in Figure 6. The driving cycles are provided to the leader vehicle via the 6G-V2X channel as the velocity profile in the platoon. Instantaneous velocities of HEVs are shared over 6G-V2V communication, where we examine how the followers react to the speed change of their leader in the platoon from the perspectives of reference velocity following, SOC charge sustainability, and fuel consumption as the ultimate goal. The research ideas of this article are demonstrated in Figure 4.

The following part presents the results of four simulation scenarios under NEDC, WLTP, HWFET, and HIL drive cycles so that the driving and energy-saving performances of connected vehicles can be validated in the platoon.

5.1. Driving performance verification results of CACC-ECMS scheme under NEDC, WLTP, HWFET, and HIL driving cycles

In this section, the effectiveness of the CACC-ECMS driving performance, which includes reference speed deviation of the follower vehicles with respect to the preceding vehicles, is assessed. Since the speed trajectory following is an important evaluation index in the platoon, we aim to minimize the deviations of the velocity between vehicles, therefore ensuring string stability. Figures 7–10 show the reference speed trajectory deviations of the vehicles in the platoon under NEDC, WLTP, HWFET, and HIL driving cycles. In Figure 7, we can observe the velocity fluctuations of the follower vehicles with respect to their leader vehicles using three different car-following models. One observation made is that the GHR-based CACC-ECMS model performs better under NEDC cooperative driving cycle than the OVM- and IDM-based CACC-ECMS schemes. How-

Figure 7. Speed profiles of car following models under NEDC driving cycle.
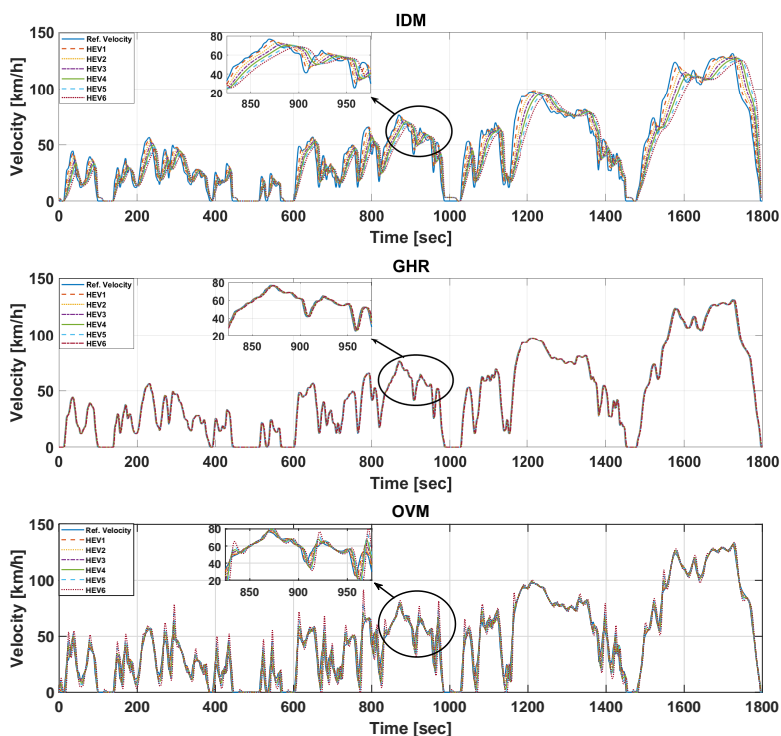
Figure 8. Speed profiles of car following models under WLTP driving cycle.

ever, the GHR- and OVM-based CACC-ECMS methods put more effort than the IDM-based CACC-ECMS method into car-following; thus, HEVs consume more fuel in the platoon, as shown in Table 3. Similarly
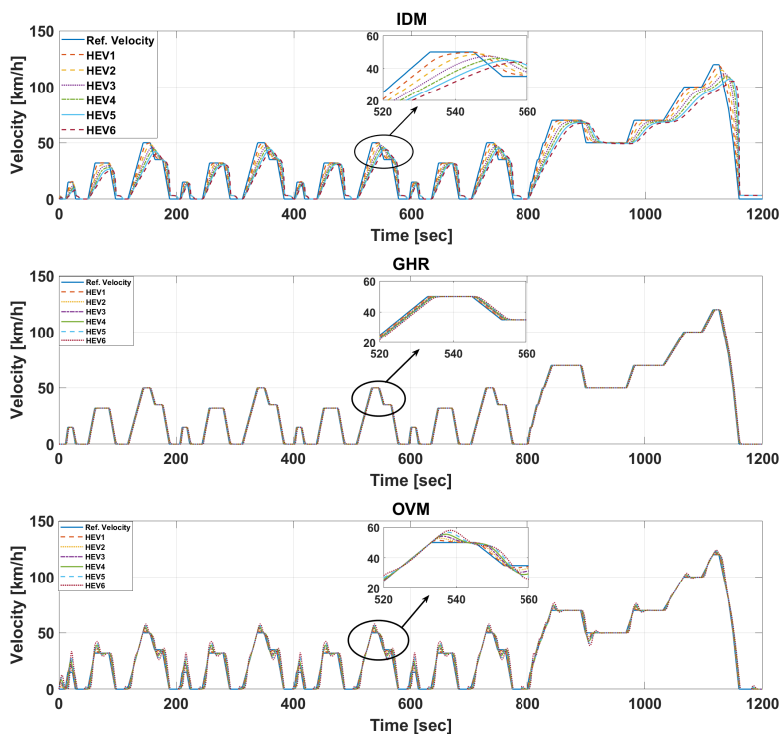
Figure 9. Speed profiles of car following models under HWFET driving cycle.

Figure 10. Speed profiles of car following models under HIL driving cycle.

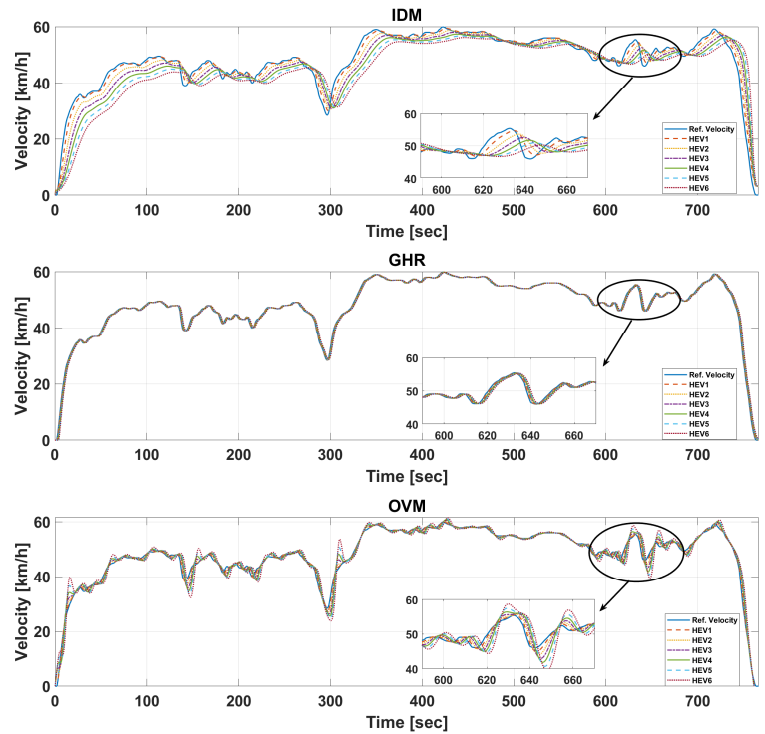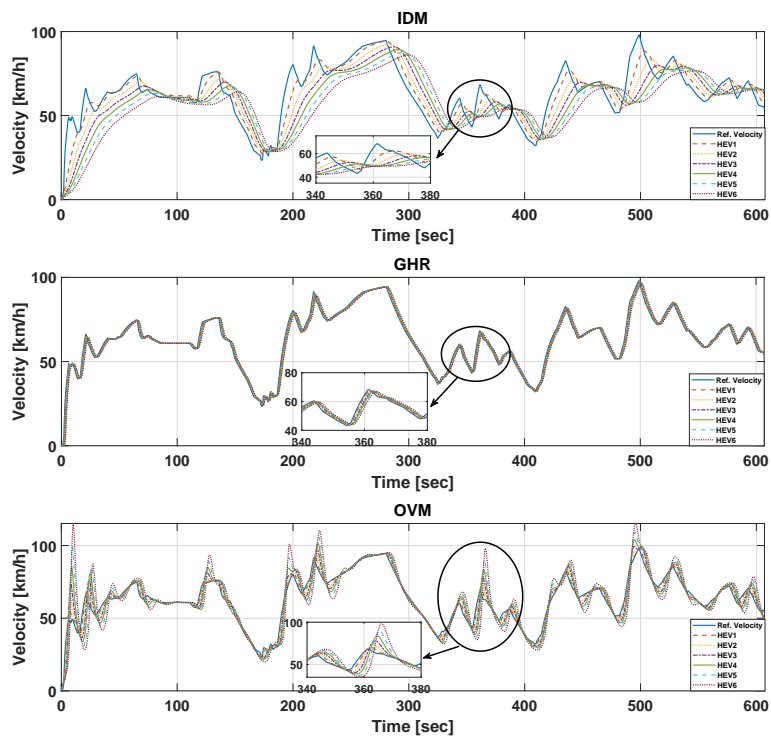results are seen in Figures 8 and 9. In Figure 8, the GHR- and OVM-based CACC-ECMS schemes perform better in the car-following mode than that of the IDM-based CACC-ECMS method, as zoomed in the figure.
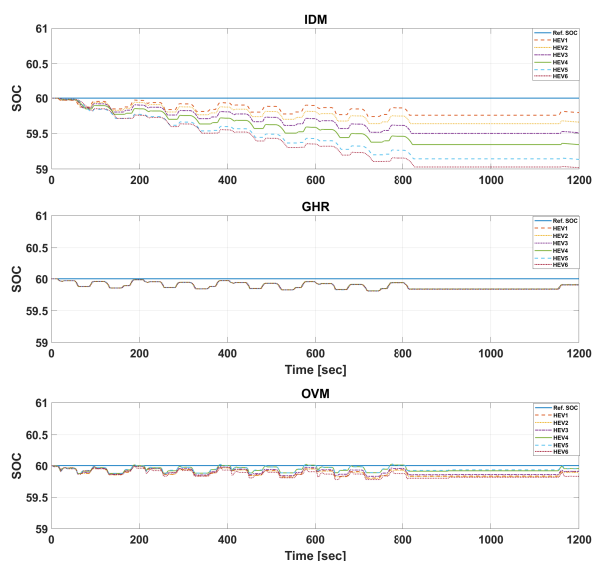
Figure 11. NEDC drive cycle SOC graph.
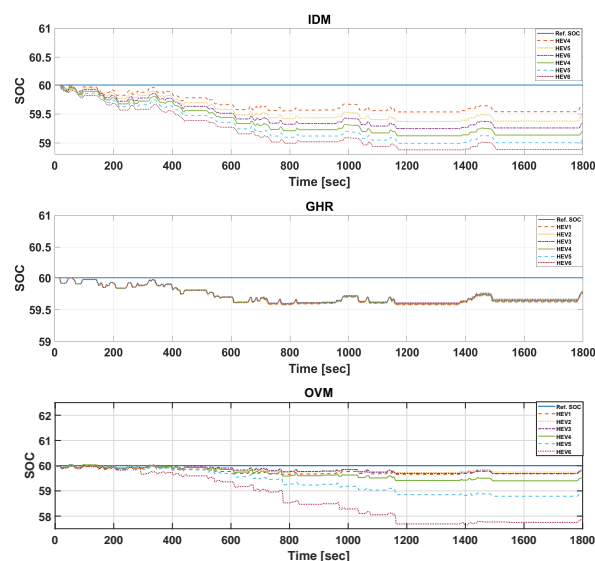
Figure 12. WLTP drive cycle SOC graph.

The tradeoff between cooperative driving performance and fuel economy exists under WLTP cycle as well. To show this, the CACC-ECMS scheme results for each car-following model are illustrated under HWFET cycle. In Figure 9, the GHR- and OVM-based CACC-ECMS schemes perform relatively well compared to the IDM-based CACC-ECMS case, where its fuel economy performance is the best in this case as well. The design is also tested in a driving simulator, dSPACE software, which is a high-fidelity driving simulator to test and validate the proposed approach. To this end, a human-in-the-loop driving simulator is an immediate and economical solution to explore the energy-saving potentials of a cooperative hybrid electric vehicle platoon under the presence of a leader vehicle driver style. The simulator is demonstrated in Figure 5. The driver controls the steering wheel, the throttle pedal, and the braking pedal. In the environment, a straight road cooperative driving condition is created, where the human driver controls the leader vehicle and six HEV followers are in the platoon for a driving test. As shown in Figure 10, the GHR- and OVM-based CACC-ECMS schemes perform better in the car-following mode than that of the IDM-based CACC-ECMS method, as zoomed in the same figure. It is seen that driver's speed profile is fluctuating; thus, the follower HEVs cannot effectively track the velocity trajectory of the preceding HEV using the IDM. It is worth noting that the tradeoff between cooperative driving performance and fuel economy exists under this cycle as well.

Some conclusions can be drawn as follows: (i) The tradeoff between reference velocity following of followers versus the fuel consumption of the platoon shows that the driving performance metric is conflicted with the consumed fuel in the platoon; (ii) Even though the GHR-based CACC-ECMS method represents the best driving performance in terms of the reference speed trajectory following, we cannot state its fuel economy is the worst because the fuel economy is also affected by the different model parameters of the proposed scheme.

5.2. Energy saving performance verification results of CACC-ECMS scheme under NEDC, WLTP, HWFET, HIL driving cycles

The effectiveness of the CACC-ECMS scheme is evaluated for energy-saving potential in the platoon in this section. Figures 11–14 show the SOC trajectory deviations of the vehicles in the platoon under NEDC, WLTP, and HWFET driving cycles. The SOC initial value, which is 60%, is to be sustained over the entire driving cycle. Figure 11 shows that the SOC levels with GHR and OVM models are closer to the reference level for each HEV under NEDC cycle in the platoon. We can also observe end-of-cycle SOC values in Table 4. This is indeed a
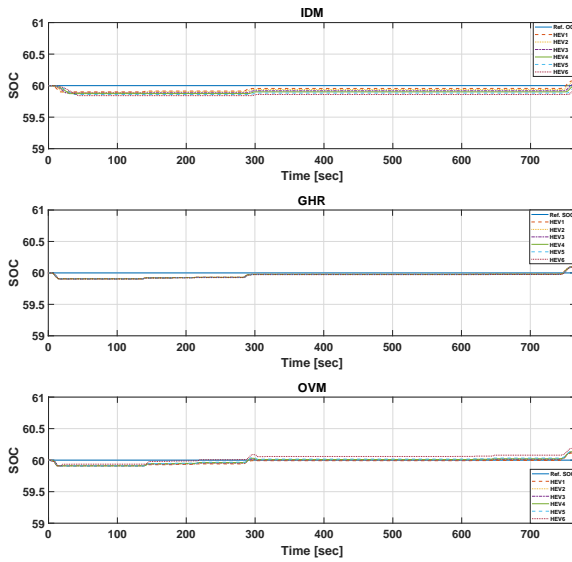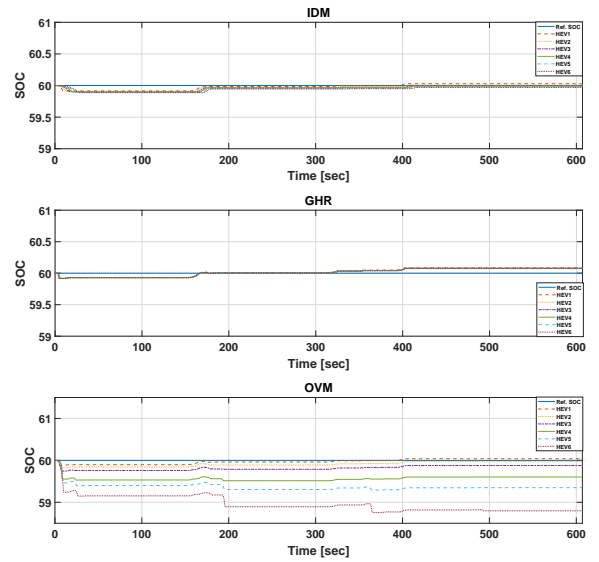
Figure 13. HWFET drive cycle SOC graph.

Figure 14. HIL drive cycle SOC graph.

good indicator of the proposed scheme, especially in terms of predictability of its trajectory using GHR and OVM models under NEDC drive cycle, so that the battery works in low resistance. One drawback of this approach is that the fuel economy is deteriorated for the members of the platoon as compared with using IDM under the same drive cycle, as seen in Table 3. The platoon fuel economy per 100 km (L/100 km) is 16.59 L using IDM, while it is 18.09 and 18.53 L using GHR and OVM, respectively. Figure 12 represents SOC findings using the CACC-ECMS scheme under WLPT drive cycle. We can observe that, similar to the NEDC case, the GHR and OVM models exhibit close values to the reference SOC level, while SOC level fluctuates around the reference level using IDM. However, the IDM-based CACC-ECMS scheme presents better fuel-saving, i.e., 17.33 L/100 km, while it is 18.73 and 19.47 L /100 km using GHR and OVM, respectively, in the platoon. Table 3 presents each HEV fuel consumption using different car-following models, subsequently global fuel-savings in the platoon. We can also observe end-of-cycle SOC values using the GHR-based CACC-ECMS scheme in Table 4. SOC trajectories of the proposed CACC-ECMS scheme under HWFET drive cycle are illustrated in Figure 13. Since HWFET cycle is a standard highway, we expect the battery SOC level to be maintained closer to the reference value, as seen in the figure. Even though all car-following models present a similar pattern, only the IDM-based SOC level deviates around the reference level for each HEV in the platoon. Similar to the previous cases, the fuel economy result of the IDM-based CACC-ECMS scheme shows improvements among the HEVs and the platoon relative to the other cases. For this driving cycle, the platoon fuel economy per 100 km (L/100 km) is 9.403 L using IDM, while it is 9.756 and 9.817 L using GHR and OVM, respectively. Lastly, SOC trajectories of the proposed CACC-ECMS scheme under HIL drive cycle are illustrated in Figure 14. The figure shows that the SOC levels deviate around the reference level for each HEV in the platoon only in the OVM case. The fluctuations in the speed profile deteriorate the string stability and energy consumption of HEVs in the platoon. In this aspect, for this driving cycle, the platoon fuel economy per 100 km (L/100 km) is 15.22 L using IDM, while it is 17.11 and 18.62 L using GHR and OVM, respectively.

One main conclusion can be drawn for all cases: the IDM-based CACC-ECMS scheme provides the best fuel economy, while there are tradeoffs for the SOC reference trajectory following performance under various drive cycles. The GHR-based CACC-ECMS scheme performs relatively better than the OVM-based scheme for energy-saving, and both methods present a similar SOC trajectory following performance under NEDC and HWFET drive cycles.

Table 3. Fuel consumption table of HEVs under different driving cycles

Drive cycle	Car Following Model	HEV	Fuel consumption (L)	The amount of fuel consumed per 100 km (L/100 km)	Drive Cycle	Car Following Model	HEV	Fuel consumption (L)	The amount of fuel consumed per) 100 km (L/100 km)
NEDC	IDM	HEV1	0.327	2.972	HWFET	IDM	HEV1	0.267	1.623
		HEV2	0.317	2.881			HEV2	0.263	1.598
		HEV3	0.308	2.799			HEV3	0.259	1.574
		HEV4	0.299	2.718			HEV4	0.256	1.556
		HEV5	0.291	2.645			HEV5	0.252	1.531
		HEV6	0.283	2.572			HEV6	0.249	1.513
		Platoon	1.825	16.59			Platoon	1.547	9.403
	GHR	HEV1	0.332	3.018		GHR	HEV1	0.268	1.629
		HEV2	0.332	3.018			HEV2	0.268	1.629
		HEV3	0.332	3.018			HEV3	0.268	1.629
		HEV4	0.331	3.009			HEV4	0.267	1.623
		HEV5	0.331	3.009			HEV5	0.267	1.623
		HEV6	0.331	3.009			HEV6	0.267	1.623
		Platoon	1.991	18.09			Platoon	1.605	9.756
	OVM	HEV1	0.333	3.027		OVM	HEV1	0.267	1.623
		HEV2	0.334	3.036			HEV2	0.268	1.629
		HEV3	0.337	3.063			HEV3	0.268	1.629
		HEV4	0.340	3.091			HEV4	0.269	1.635
		HEV5	0.346	3.145			HEV5	0.270	1.641
		HEV6	0.347	3.154			HEV6	0.271	1.647
		Platoon	2.039	18.53			Platoon	1.615	9.817
WLTP	IDM	HEV1	0.715	3.075	HIL	IDM	HEV1	0.289	2.711
		HEV2	0.694	2.984			HEV2	0.279	2.617
		HEV3	0.677	2.911			HEV3	0.272	2.551
		HEV4	0.661	2.843			HEV4	0.267	2.504
		HEV5	0.647	2.782			HEV5	0.261	2.448
		HEV6	0.635	2.731			HEV6	0.255	2.392
		Platoon	4.030	17.33			Platoon	1.623	15.22
	GHR	HEV1	0.727	3.126		GHR	HEV1	0.306	2.869
		HEV2	0.726	3.122			HEV2	0.305	2.861
		HEV3	0.726	3.122			HEV3	0.304	2.851
		HEV4	0.725	3,117			HEV4	0.304	2.851
		HEV5	0.725	3,117			HEV5	0.303	2.842
		HEV6	0.725	3,117			HEV6	0.302	2.833
		Platoon	4.355	18.73			Platoon	1.825	17.11
	OVM	HEV1	0.732	3.148		OVM	HEV1	0.311	2.917
		HEV2	0.739	3.178			HEV2	0.317	2.973
		HEV3	0.748	3.217			HEV3	0.324	3.039
		HEV4	0.756	3.251			HEV4	0.332	3.114
		HEV5	0.769	3.307			HEV5	0.343	3.217
		HEV6	0.785	3.376			HEV6	0.356	3.335
		Platoon	4.529	19.47			Platoon	1.985	18.62

6. CONCLUSION

This work proposes a hybrid electric vehicle (HEV) platoon control using car-following model-based cooperative adaptive cruise control (CACC). Utilizing sixth-generation vehicle-to-everything (6G-V2X) communications network service for connected and automated HEV platoon, HEVs are capable of communicating with the base station to receive target traffic states such as reference velocities and positions. Using the obtained traffic data, an equivalent consumption minimization strategy (ECMS) is used for power flow management, where the velocities of leader vehicles are used for cooperative driving as well as energy-saving. With the help of the predecessor-following communication topology in the platoon, the proposed CACC-ECMS framework fully explores the advantage of fuel consumption reduction while ensuring string stability. Experiments under different drive cycles result in the following conclusions:

- The GHR- and OVM-based CACC-ECMS schemes present better car-following performance than that of the IDM-based CACC-ECMS scheme at the cost of fuel consumption.
- The SOC reference trajectory following performance of the GHR- and OVM-based CACC-ECMS schemes is better in terms of target deviation over the entire drive cycles than that of the IDM-based CACC-ECMS

Table 4. End-of-cycle SOC values of HEVs under different driving cycles

Drive Cycle	Car Following Model	HEV	SOC(%)	Drive Cycle	Car Following Model	HEV	SOC(%)
NEDC	IDM	HEV1	59.81	HWFET	IDM	HEV1	60.08
		HEV2	59.68			HEV2	60.05
		HEV3	59.53			HEV3	60.01
		HEV4	59.35			HEV4	59.99
		HEV5	59.14			HEV5	59.95
		HEV6	59.02			HEV6	59.92
	GHR	HEV1	59.91		GHR	HEV1	60.10
		HEV2	59.91			HEV2	60.10
		HEV3	59.91			HEV3	60.10
		HEV4	59.91			HEV4	60.10
		HEV5	59.90			HEV5	60.10
		HEV6	59.90			HEV6	60.09
	OVM	HEV1	59.89		OVM	HEV1	60.11
		HEV2	59.89			HEV2	60.12
		HEV3	59.91			HEV3	60.13
		HEV4	59.95			HEV4	60.13
		HEV5	59.95			HEV5	60.13
		HEV6	59.96			HEV6	60.17
WLTP	IDM	HEV1	59.67	HIL	IDM	HEV1	60.03
		HEV2	59.49			HEV2	60.01
		HEV3	59.35			HEV3	60.00
		HEV4	59.20			HEV4	59.99
		HEV5	59.05			HEV5	59.98
		HEV6	58.91			HEV6	59.97
	GHR	HEV1	59.77		GHR	HEV1	60.09
		HEV2	59.76			HEV2	60.08
		HEV3	59.75			HEV3	60.08
		HEV4	59.75			HEV4	60.08
		HEV5	59.74			HEV5	60.08
		HEV6	59.74			HEV6	60.07
	OVM	HEV1	59.86		OVM	HEV1	60.04
		HEV2	59.85			HEV2	59.97
		HEV3	59.79			HEV3	59.88
		HEV4	59.49			HEV4	59.60
		HEV5	58.87			HEV5	59.35
		HEV6	57.84			HEV6	58.80

approach.

- In the platoon, the IDM-based CACC-ECMS consumes fuel at 16.59 L/100 km under NEDC, 17.33 L/100 km under WLTP, 9.403 L/100 km under HWFET, and 15.22 L/100 km under HIL. The GHR-based CACC-ECMS consumes fuel at 18.09 L/100 km under NEDC, 18.73 L/100 km under WLTP, 9.756 L/100 km under HWFET, and 17.11 L/100 km under HIL. The OVM-based CACC-ECMS consumes fuel at 18.53 L/100 km under NEDC, 19.47 L/100 km under WLTP, 9.817 L/100 km under HWFET, and 18.62 L/100 km under HIL.
- The IDM-based CACC-ECMS is an energy-efficient strategy that saves: (i) 8.29% fuel compared to the GHR-based CACC-ECMS and 10.47% compared to the OVM-based CACC-ECMS under NEDC; (ii) 7.47% fuel compared to the GHR-based CACC-ECMS and 11% compared to the OVM-based CACC-ECMS under WLTP; (iii) 3.62% fuel compared to the GHR-based CACC-ECMS and 4.22% compared to the OVM-based CACC-ECMS under HWFET; and (iv) 11.05% fuel compared to the GHR-based CACC-ECMS and 18.26% compared to the OVM-based CACC-ECMS under HIL.

Future work will be directed toward the influence of the interaction of vehicles on energy-saving potentials. The negative impacts of communication outage on energy-saving deterioration will also be investigated.

Symbols and abbreviations in the article are given in Table 5.

Table 5. Symbols and abbreviations

Symbols			
$\dot{m}_{eqv}$	Equivalent fuel consumption	C	Carrier gear
$\dot{m}_{fuel}$	Engine fuel consumption	R	Ring gear
$\dot{x}_0$	Desired velocity of the vehicle nth	S	Sun gear
$\ddot{x}_n$	Acceleration of the nth vehicle nth	T	Safe time headway
$\dot{x}_n$	Velocity of the nth vehicle	T_m	Electric motor torque
Ψ_{eng}	Engine empirical data	b	Maximum deceleration
$\Psi_{M/G1}$	Generator empirical data	g	Gravitational acceleration
$\Psi_{M/G2}$	Motor empirical data	m	Vehicle mass
C_d	Rolling resistance coefficient	n_m	Electric motor speed
I_{batt}	Battery current	s	Equivalent factor
$I_{M/G1}$	Generator inertia	α	Engine throttle
$I_{M/G2}$	Motor inertia	δ	Exponent for vehicle's acceleration
I_{eng}	Engine inertia	θ	Road grade
g_f	Gear ratio of final drive	Abbrevations	
P_{batt}	Battery power	ACC	Adaptive cruise control
P_m	Electric motor power	CACC	Cooperative adaptive cruise control
Q_{max}	Capacity of battery	CAV	Connected and automated vehicle
R_{batt}	Internal resistance	ECMS	Equivalent consumption minimization strategy
R_{wheel}	Radius of wheel	EF	Equivalent factor
T_{axle}	Axle torque	EM	Electric motor
T_{brake}	Brake torque	EMS	Energy management system
T_e	Engine torque	GHR	Gazis–Herman–Rothery model
T_{emax}	Engine maximum torque	HEV	Hybrid electric vehicle
V_{oc}	Open circuit voltage	HWFET	Highway fuel economy test
l_n	Vehicle length	ICE	Internal combustion engine
n_e	Engine speed	IDM	Intelligent driver model
s_0	Minimum space	ITS	Intelligent transportation system
η_{inv}	Inverter efficiency	MPC	Model predictive control
η_m	Electric motor efficiency	NEDC	New European driving cycle
ω_C	Carrier gear angular velocity	OVM	Optimal velocity model
ω_{eng}	Engine angular speed	PMP	Pontryagin's minimum principle
$\omega_{M/G1}$	$M/G1$ angular speed	SOC	State of charge
$\omega_{M/G2}$	$M/G2$ angular speed	V2I	Vehicle-to-infrastructure
ω_R	Ring gear angular velocity	V2V	Vehicle-to-vehicle
ω_S	Sun gear angular velocity	V2X	Vehicle-to-everything
$\Delta\dot{x}_n$	Distance between vehicles	WLTP	Worldwide harmonized light vehicles test procedure
N	number of vehicles in platoon	6G	sixth generation
F	Internal force on pinion gears	6G-V2X	sixth-generation vehicle-to-everything

DECLARATIONS

Acknowledgments

The authors would like to thank the anonymous reviewers for their valuable comments.

Authors' contributions

Made substantial contributions to conception, manuscript preparation, experimental studies, and manuscript editing/revision: Yazar O, Coskun S
Made substantial contributions to reviewing/editing and technical notes: Zhang F, Li L

Availability of data and materials

Not applicable.

Financial support and sponsorship

Conflicts of interest

All authors declared that there are no conflicts of interest.

Ethical approval and consent to participate
Not applicable.

Consent for publication
Not applicable.

Copyright

REFERENCES

1. Saiteja P, Ashok B. Critical review on structural architecture, energy control strategies and development process towards optimal energy management in hybrid vehicles. *Energy Reviews* 2022;157:112038 https://doi.org/10.1016/j.rser.2021.112038.
2. Zhang F, Hu X, Langari R, Cao D. Energy management strategies of connected hevs and phevs: Recent progress and outlook. *Progress in Energy and Combustion Science* 2019;73:235-56. https://doi.org/10.1016/j.pecs.2019.04.002.
3. Li L, Coskun S, Wang J, Fan Y, Zhang F, Langari R. Velocity prediction based on vehicle lateral risk assessment and traffic flow: A brief review and application examples. *Energies* 2021;14:3431. https://doi.org/10.3390/en14123431.
4. Yadlapalli RT, Kotapati A, Kandipati R, Koritala CS. A review on energy efficient technologies for electric vehicle applications. *J Energy Storage* 2022;50:104212. https://doi.org/10.1016/j.est.2022.104212.
5. Ruan S, Ma Y, Yang N, Xiang C, Li X. Real-time energy-saving control for HEVs in car-following scenario with a double explicit MPC approach. *Energy* 2022;247:123265. https://doi.org/10.1016/j.energy.2022.123265.
6. Hu X, Wang H, Tang X. Cyber-physical control for energy-saving vehicle following with connectivity. *IEEE Trans Ind Electron* 2017;64:8578-87. 2017. https://doi.org/10.1109/TIE.2017.2703673.
7. Kannan Chidambaram, Bragadeshwaran Ashok, Rajasekar Vignesh, Chirag Deepak, Rathan Ramesh, Tharun MV Narendhra, Kaisan Muhammad Usman, and Chellapan Kavitha. Critical analysis on the implementation barriers and consumer perception toward future electric mobility. *Proceedings of the Institution of Mechanical Engineers, Part D: Journal of Automobile Engineering*, page 09544070221080349, 2022. https://doi.org/10.1177%2F09544070221080349.
8. Liu Z, Lee H, Khyam M, et al. 6g for vehicle-to-everything (v2x) communications: Enabling technologies, challenges, and opportunities. *arXiv preprint arXiv:2012.07753*, 2020. https://doi.org/10.48550/arXiv.2012.07753.
9. Prathiba SB, Raja G, Kumar N. Intelligent cooperative collision avoidance at overtaking and lane changing maneuver in 6g-v2x communications. *IEEE Trans Veh Technol* 2022;71:112-22. https://doi.org/10.1109/TVT.2021.3127219.
10. Yang C, Zha M, Wang W, Liu K, Xiang C. Efficient energy management strategy for hybrid electric vehicles/plug-in hybrid electric vehicles: review and recent advances under intelligent transportation system. *IET Intelligent Transport Systems* 2020;14:702-11. https://doi.org/10.1049/iet-its.2019.0606.
11. He H, Wang Y, Han R, Han M, Bai Y, Liu Q. An improved mpc-based energy management strategy for hybrid vehicles using v2v and v2i communications. *Energy* 2021;225:120273. https://doi.org/10.1016/j.energy.2021.120273.
12. Zhao Z, Tang P, Li H. Generation, screening, and optimization of powertrain configurations for power-split hybrid electric vehicle: A comprehensive overview. *IEEE Trans Transp Electrific* 2022;8:325-44. https://doi.org/10.1109/TTE.2021.3105244.
13. Kannan C, Vignesh R, Karthick C, Ashok B. Critical review towards thermal management systems of lithium-ion batteries in electric vehicle with its electronic control unit and assessment tools. *Proceedings of the Institution of Mechanical Engineers, Part D: Journal of Automobile Engineering* 2021;235:1783-807. https://doi.org/10.1177%2F09544070209828651O.1177/0954407020982865.
14. Zhang F, Wang L, Coskun S, Pang H, Cui Y, Xi J. Energy management strategies for hybrid electric vehicles: Review, classification, comparison, and outlook. *Energies* 2020;13:3352. https://doi.org/10.3390/en13133352.
15. Vignesh R, Ashok B. Deep neural network model-based global calibration scheme for split injection control map to enhance the characteristics of biofuel powered engine. *Energy Conversion and Management* 2021;249:114875. https://doi.org/10.1016/j.enconman.2021.114875.
16. Omanovic A, Zsiga N, Soltic P, Onder C. Optimal degree of hybridization for spark-ignited engines with optional variable valve timings. *Energies* 2021;14:8151. https://doi.org/10.3390/en14238151.
17. Onori S, Serrao L, Rizzoni G. Hybrid electric vehicles: Energy management strategies. 2016.
18. Liu T, Tan W, Tang X, Zhang J, Xing Y, Cao D. Driving conditions-driven energy management strategies for hybrid electric vehicles: A review. *Renewable and Sustainable Energy Reviews* 2021;151:111521. https://doi.org/10.1016/j.rser.2021.111521.
19. Paganelli G. Design and control of a parallel hybrid car with electric and thermal powertrain. *M. Sc*, 1999.
20. Shi D, Liu S, Cai Y, Wang S, Li H, Chen L. Pontryagin's minimum principle based fuzzy adaptive energy management for hybrid electric vehicle using real-time traffic information. *Applied Energy* 2021;286:116467. https://doi.org/10.1016/j.apenergy.2021.116467.
21. Zhang F, Xiao L, Coskun S, et al. Comparative study of energy management in parallel hybrid electric vehicles considering battery ageing. *Energy* 2022;123219. https://doi.org/10.1016/j.energy.2022.123219.
22. Zhang F, Xi J, Langari R. Real-time energy management strategy based on velocity forecasts using v2v and v2i communications. *IEEE Trans Intell Transport Syst* 2017;18:416-30. https://doi.org/10.1109/TITS.2016.2580318.
23. Deshpande SR, Jung D, Bauer L, Canova M. Integrated approximate dynamic programming and equivalent consumption minimization

strategy for eco-driving in a connected and automated vehicle. *IEEE Trans Veh Technol* 2021;70:11204-15. https://doi.org/10.1109/TVT.2021.3102505.

24. Wang W, Guo X, Yang C, et al. A multi-objective optimization energy management strategy for power split hev based on velocity prediction. *Energy* 2022;238:121714. https://doi.org/10.1016/j.energy.2021.121714.

25. Chen Z, Liu Y, Ye M, Zhang Y, Chen Z, Li G. A survey on key techniques and development perspectives of equivalent consumption minimisation strategy for hybrid electric vehicles. *Renewable and Sustainable Energy Reviews* 2021;151:111607. https://doi.org/10.1016/j.rser.2021.111607.

26. Guanetti J, Kim Y, Borrelli F. Control of connected and automated vehicles: state of the art and future challenges. *Annual Reviews in Control* 2018;45:18-40. https://doi.org/10.1016/j.arcontrol.2018.04.011.

27. Homchaudhuri B, Lin R, Pisu P. Hierarchical control strategies for energy management of connected hybrid electric vehicles in urban roads. *Transportation Research Part C: Emerging Technologies* 2016;62:70-86. https://doi.org/10.1016/j.trc.2015.11.013.

28. Pipes LA. An operational analysis of traffic dynamics. *Journal of Applied Physics* 1953;24:274-81. https://doi.org/10.1063/1.1721265.

29. Chandler RE, Herman R, Montroll EW. Traffic dynamics: studies in car following. *Operations Research* 1958;6:165-84. https://doi.org/10.1287/opre.6.2.165.

30. Treiber M, Hennecke A, Helbing D. Congested traffic states in empirical observations and microscopic simulations. *Phys Rev E Stat Phys Plasmas Fluids Relat Interdiscip Topics* 2000;62:1805-24. https://doi.org/10.1103/PhysRevE.62.1805.

31. Gazis DC, Herman R, Rothery RW. Nonlinear follow-the-leader models of traffic flow. *Operations Research* 1961;9:545-67. https://doi.org/10.1287/opre.9.4.545.

32. Bando M, Hasebe K, Nakayama A, Shibata A, Sugiyama Y. Dynamical model of traffic congestion and numerical simulation. *Phys Rev E Stat Phys Plasmas Fluids Relat Interdiscip Topics* 1995;51:1035-42. https://doi.org/10.1103/PhysRevE.51.1035.

33. Ioannou P, Chien C. Autonomous intelligent cruise control. *IEEE Trans Veh Technol* 1993;42:657-72. https://doi.org/10.1109/25.260745.

34. Fellendorf M, Vortisch P. Microscopic traffic flow simulator vissim. In: Barceló J, editor. Fundamentals of Traffic Simulation. New York: Springer; 2010. pp. 63-93. https://doi.org/10.1007/978-1-4419-6142-6_2.

35. Li G, Gorges D. Ecological adaptive cruise control and energy management strategy for hybrid electric vehicles based on heuristic dynamic programming. *IEEE Trans Intell Transport Syst* 2019;20:3526-35. https://doi.org/10.1109/TITS.2018.2877389.

36. Vajedi M, Azad NL. Ecological adaptive cruise controller for plug-in hybrid electric vehicles using nonlinear model predictive control. *IEEE Trans Intell Transport Syst* 2016;17:113-22. https://doi.org/10.1109/TITS.2015.2462843.

37. Jia Y, Jibrin R, Gorges D. Energy-optimal adaptive cruise control for electric vehicles based on linear and nonlinear model predictive control. *IEEE Trans Veh Technol* 2020;69:14173-87. https://doi.org/10.1109/TVT.2020.3044265.

38. Ma G, Ghasemi M, Song X. Integrated powertrain energy management and vehicle coordination for multiple connected hybrid electric vehicles. *IEEE Trans Veh Technol* 2018;67:2893-9. https://doi.org/10.1109/TVT.2017.2780268.

39. Li J, Zhou Q, He Y, Williams H, Xu H, Lu G. Distributed cooperative energy management system of connected hybrid electric vehicles with personalized non-stationary inference. *IEEE Trans Transp Electrific* 2022;8:2996-3007. https://doi.org/10.1109/TTE.2021.3127142.

40. Ma F, Yang Y, Wang J, et al. Predictive energy-saving optimization based on nonlinear model predictive control for cooperative connected vehicles platoon with v2v communication. *Energy* 2019;189:116120. https://doi.org/10.1016/j.energy.2019.116120.

41. Xu L, Zhuang W, Yin G, Bian C. Energy-oriented cruising strategy design of vehicle platoon considering communication delay and disturbance. *Transportation Research Part C: Emerging Technologies* 2019;107:34-53. https://doi.org/10.1016/j.trc.2019.07.019.

42. Syed FU, Kuang ML, Czubay J, Ying H. Derivation and experimental validation of a power-split hybrid electric vehicle model. *IEEE Trans Veh Technol* 2006;55:1731-47. https://doi.org/10.1109/TVT.2006.878563.

43. Liu J, Peng H. Modeling and control of a power-split hybrid vehicle. *IEEE Trans Contr Syst Technol* 2008;16:1242-51 https://doi.org/10.1109/TCST.2008.919447.

44. Yang Y, Hu X, Pei H, Peng Z. Comparison of power-split and parallel hybrid powertrain architectures with a single electric machine: Dynamic programming approach. *Applied Energy* 2016;168:683-90. https://doi.org/10.1016/j.apenergy.2016.02.023.

45. Sun C, Hu X, Moura SJ, Sun F. Velocity predictors for predictive energy management in hybrid electric vehicles. *IEEE Trans Contr Syst Technol* 2015;23:1197-204. https://doi.org/10.1109/TCST.2014.2359176.

46. Sun C, Sun F, He H. Investigating adaptive-ecms with velocity forecast ability for hybrid electric vehicles. *Applied Energy* 2017;185:1644-53. https://doi.org/10.1016/j.apenergy.2016.02.026.

47. Hu X, Li S, Peng H. A comparative study of equivalent circuit models for li-ion batteries. *Journal of Power Sources* 2012;198:359-67. https://doi.org/10.1016/j.jpowsour.2011.10.013.

48. Moura SJ, Chaturvedi NA, Krstić M. Adaptive partial differential equation observer for battery state-of-charge/state-of-health estimation via an electrochemical model. *Journal of Dynamic Systems, Measurement, and Control* 2014;136:011015. https://doi.org/10.1115/1.4024801.

49. Muta K, Yamazaki M, Tokieda J. Development of new-generation hybrid system ths ii-drastic improvement of power performance and fuel economy. Technical report, 2004. https://doi.org/10.4271/2004-01-0064.

50. Rousseau A, Kwon J, Sharer P, Pagerit S, Duoba M. Integrating data, performing quality assurance, and validating the vehicle model for the 2004 prius using psat. Technical report, SAE Technical Paper, 2006. https://doi.org/10.4271/2006-01-0667.

51. Treiber M, Kesting A. Traffic flow dynamics. *Traffic Flow Dynamics: Data, Models and Simulation, Springer-Verlag Berlin Heidelberg*, 2013. http://dx.doi.org/10.1007/978-3-642-32460-4.

52. Gipps P. A behavioural car-following model for computer simulation. *Transportation Research Part B: Methodological* 1981;15:105-11. https://doi.org/10.1016/0191-2615(81)90037-0.

53. Brackstone M, Mcdonald M. Car-following: a historical review. *Transportation Research Part F: Traffic Psychology and Behaviour* 1999;2:181-96. https://doi.org/10.1016/S1369-8478(00)00005-X.

54. Jiang R, Wu Q, Zhu Z. Full velocity difference model for a car-following theory. *Phys Rev E Stat Nonlin Soft Matter Phys* 2001;64:017101. https://doi.org/10.1103/PhysRevE.64.017101.

55. Treiterer J, Myers J. The hysteresis phenomenon in traffic flow. *Transportation and traffic theory*, 6:13–38, 1974. .

56. Rahman M, Chowdhury M, Dey K, Islam MR, Khan T. Evaluation of driver car-following behavior models for cooperative adaptive cruise control systems. *Transportation Research Record* 2017;2622:84-95. https://doi.org/10.3141%2F2622-08.